# Influence of seal compliance on the dynamics of an unbalanced rotor

Simon Bäuerle, Hartmut Hetzler

# Influence of seal compliance on the dynamics of an unbalanced rotor

Simon Bäuerle [1]*, Hartmut Hetzler[1]

ISROMAC 2017

International Symposium on Transport Phenomena and Dynamics of Rotating Machinery

Maui, Hawaii

December 16-21, 2017

**Abstract**

Compliant hybrid seals offer a comparatively new approach to reduce leakage in turbo machinery, leading to higher efficiency even under transient operation. These properties are achieved by a reduced sealing gap along with added seal flexibility to minimize the risk of surface rubbing. This contribution investigates the rotordynamic properties by means of a minimal model consisting of a *Jeffcott* rotor and a visco-elastically supported seal. The steady state stability, the bifurcation behavior and the resulting limit cycles of an unbalanced rotor are being discussed and compared to the results for a balanced rotor and the case of a stiff seal support. The compliant support can either enlarge or reduce the stable operation range depending on design parameters. The permitted seal movability minimizes the risk of rotor-seal contact during passage through the resonance. Rotor and seal orbits induced by unbalance can loose their stability via *Neimark-Sacker* bifurcations but then also resynchronize.

**Keywords**

rotordynamic — seal — hybrid – unbalance – Hopf bifurcation – Neimark-Sacker bifurcation

[1] *Department of Mechanics - Engineering Dynamics, University of Kassel, Kassel, Germany*

*__Corresponding author__: baeuerle@uni-kassel.de

## 1. INTRODUCTION

Seals are important components to reduce leakage in all kinds of rotating machinery and have been used for a long time. Still, these seemingly simple elements face new design challenges ranging from the demand for higher efficiency to the demand for long inspection intervals.

In present industrial practice, the mainly used seals for rotordynamic application are labyrinth and brush seals. Labyrinth seals are comparatively inexpensive and in theory wear-free. In practice, though, rotor-seal contact is not uncommon [2] resulting in decreased leakage performance. The fluid flow through the seal leads to cross-coupled stiffnesses and, therefore, rotordynamic instabilities above a certain threshold speed. Instabilities can be shifted to higher rotational speeds by surface texturing or swirl brakes [3] but not entirely be prevented. Brush seals on the contrary can further reduce leakage and adapt to shaft movement [4]. Rotordynamic impact due to fluid forces is negligible and proper design can avoid thermally induced vibrations (Newkirk-effect [5]) by localized frictional heating. Yet, low axial stiffness and bristle wear with subsequent increased leakage [2] are challenges.

A comparatively new approach trying to combine advantages of labyrinth and brush seals are compliant hybrid seals (e.g. Halo seal [2], Gland seal [6]): a contact-free design leads to low wear while compliance in the seal structure permits rotor deflection without surface rubbing. The adaptability allows for smaller sealing gaps and, thus, lowered leakage with subsequent increased efficiency. In addition, Halo and Gland seal narrow the gap width with increasing pressure giving a rotor the needed space for movement during start-up or shut-down runs. Halo seals are already being used and can reduce leakage up to 70% compared with labyrinth seals [2].

This contribution focuses on the rotordynamic behavior under the influence of compliant seal structures employing a generic fluid forces model representing in this case an incompressible fluid. Rotor instabilities due to laminar flow in journal bearings are a long known phenomenon: *Newkirk* was one of the first to report on this in 1924 [7]. The destabilizing influence of seals wasn't investigated until the 50's when *Lomakin* amongst others published on this issue in 1957 [8]. In contrast to bearings the flow in seals is predominantly turbulent due to the comparatively large gap and due to the pressure gradient over the seal with consequential high axial velocities. Thus, the usage of *Reynolds* equations is not allowed anymore. And since coupled fluid-structure-interaction simulations with respect to the full *Navier-Stokes* equations are most of the time too costly, reduced models are required. Amongst others *Ng* and *Pan* [9], *Constantinescu* [10] and *Hirs* [11] developed such simplified models for low and high Reynolds numbers making use of the small aspect ratio between sealing gap and rotor radius. If coupled simulations with reduced models are still too cumbersome, seal forces can alternatively be represented by force coefficient models stemming either from experimental measurements, full CFD simulations or an analytical derivations of the mentioned reduced models as i.e. done by *Childs* [1]. Another way is to postulate some of the dependencies of the fluid

| subscripted $R$/ $S$: rotor/seal-related | | | |
|---|---|---|---|
| $\mathcal{I}$ : inertially fixed cartesian reference frame | | $\mathcal{R}$ : rotor fixed/ co-rotating cartesian reference frame | |
| $\mathbf{q}_{R,S}$ | position vector wrt $\mathcal{R}$ | $m_0$ | *Childs-Hirs* coefficient [1] |
| $\Delta\mathbf{q} = \mathbf{q}_R - \mathbf{q}_S$ | relative rotor deflection wrt $\mathcal{R}$ | $n$ | empirical parameter |
| $\mathbf{q}_0$ | equilibrium position wrt $\mathcal{R}$ | $n_0$ | *Childs-Hirs* coefficient [1] |
| $\mathbf{r}_{R,S}$ | position vector wrt $\mathcal{I}$ | $t$ | time |
| $\Delta\mathbf{r} = \mathbf{r}_R - \mathbf{r}_S$ | relative rotor deflection wrt $\mathcal{I}$ | $C$ | nominal sealing gap |
| $\mathbf{F}_f(\Delta\mathbf{r})$ | fluid force wrt $\mathcal{I}$ | $D_f/D_{f0}$ | fluid damping |
| $\mathbf{B}_{(),R,S}$ | general/ rotor/ seal matrix of velocity proportional forces | $K_f/K_{f0}$ | fluid stiffness |
| $\mathbf{C}_{(),R,S}$ | general/ rotor/ seal matrix of position proportional forces | $L$ | seal length |
| $\mathbf{M}_{(),R,S}$ | general/ rotor/ seal mass matrix | $\eta = \frac{\Omega}{\omega_R}$ | dimensionless angular rotor speed |
| $\mathbf{Q}$ | matrix defined by equation (14) | $\kappa^2 = \frac{c_S}{c_R}$ | stiffness ratio |
| $\mathbf{R}$ | rotation matrix | $\mu$ | dynamic fluid viscosity |
| $b$ | empirical parameter | $\xi$ | *Childs-Hirs* pressure loss coefficient [1] |
| $c_{R,S}$ | stiffness coefficient | $\rho$ | fluid density |
| $d_{R,S}$ | damping coefficient | $\tau_f/\tau_{f0}$ | fluid average circumferential velocity ratio/ constant |
| $e$ | mass eccentricity | $\omega_R = \sqrt{\frac{c_R}{m_R}}$ | rotor eigenfrequency (dry critical speed) |
| $m_f$ | coefficient of fluid inertia | $\Omega$ | angular rotor speed |
| $m_{R,S}$ | rotor/ seal mass | | |

**Table 1.** Nomenclature of used variables and parameters.

| | | | | | | | | | |
|---|---|---|---|---|---|---|---|---|---|
| $b$ | = | 0.5 | $m_0$ | = | -0.25 | $C$ | = | $0.005 \cdot R$ | $d_R$ | = | 0 | $\xi$ | = | 0.5 |
| $c_R$ | = | $7.92 \cdot 10^4 \frac{\mathrm{N}}{\mathrm{m}}$ | $n$ | = | 2 | $L$ | = | $0.1 \cdot R$ | $d_S$ | = | $\frac{0.05}{2\sqrt{c_S m_S}}$ | $\rho$ | = | $1000 \frac{\mathrm{kg}}{\mathrm{m}^3}$ |
| $m_R$ | = | 50 kg | $n_0$ | = | 0.066 | $R$ | = | $15 \cdot 10^{-2}$m | $\mu$ | = | $1.295 \cdot 10^{-3} \frac{\mathrm{Ns}}{\mathrm{m}^2}$ | $\tau_0$ | = | 0.45 |
| $m_S$ | = | $0.25 \cdot m_R$ | $\Delta p$ | = | $5 \cdot 10^5 \frac{\mathrm{N}}{\mathrm{m}^2}$ | | | | | | | | | |

**Table 2.** Specific parameter values used for simulation (if not indicated otherwise).

forces i.e. on rotor speed and deflection and determine the remaining coefficient values by one of the before mentioned methods. Such a model was set up by *Muszynska* in 1986 [12].

Being able to describe the influence of the fluid a basic understanding of the dynamic phenomena in rotor/seal systems needs to be developed: simple *Jeffcott* rotor models are used frequently as a first step. *Ding* [13] used a rotor/seal model with stiff bearings and described the seal forces with the *Muszynska* model. The solution of the balanced system looses its stability in a *Hopf* bifurcation, whereas the unbalanced system shows a *Neimark-Sacker* or period doubling bifurcation depending on the level of mass eccentricity. *S. Li* [14] used the same model and found similar results. In addition, he could show the existence of reoccurring periodic windows within the quasi-periodic operation range. *W. Li*'s [15] sealed rotor is mounted in fluid film bearings and experiences an even richer dynamical behaviour, where periodic motions become double-periodic, quasi-periodic and resynchronize to periodic motions again before becoming multi-/quasi-periodic at maximum speed. All three authors used *Childs'* equations for incompressible fluid seal forces [1] to compute the parameters in the *Muszynska* model, which is also done here.

Thematically similar to a flexible seal structure or support is a flexible fluid film bearing support: More recent works like *Vázquez'* [16] could theoretically and experimentally show an increase in onset speed of instability and an increase in the first resonance amplitude with decreasing support stiffness as well as a continuance in the first and a decrease in the second critical speed with decreasing support stiffness. *Guo* and *Kirk* [17] highlighted the influence of the support damping on the onset speed of instability, stating that there is no monotonous dependence but rather a range of optimal values. *Bai* [18] investigated a FEM model of a turbopump comprising a seal and two rolling bearings, one being flexibly supported. Neglecting the compressibility of the gaseous working operating medium, they could show a significant dependence of the onset speed of instability on the support flexibility, where an intermediate stiffness lead to the highest stable operation speed.

The investigation of the influence of compliant seal structures

on rotordynamics is the topic of this contribution. Therefore, a minimal model comprising a *Jeffcott* rotor with mass eccentricity and a visco-elastically supported stiff seal ring is considered. The non-linear *Muszynska* model is used to account for the incompressible fluid forces. In the *modelling* section the equations of motion with respect to an inertially fixed reference frame and with respect to a co-rotating reference frame are derived. The *Muszynska* model is discussed. The *results* section is subdivided in three parts: At first, the solution stability is reviewed followed by a discussion on two exemplary bifurcation paths. The contribution closes with a conclusion and an outlook.

## 2. MODELLING

Figure 1 shows the used minimal model which consists of three parts: The first one is a classical *Jeffcott*-rotor: It spins with the constant angular velocity $\Omega$ and the center of mass $S$ has the eccentricity $e$. The second part is a stiff seal ring, which is visco-elastically connected to its inertially fixed surrounding. This support allows only for translative motions. The two rigid bodies move solely in-plane and their physical properties are indicated in figure 1 and the used parameter values can be found in table 2.

With respect to an inertial cartesian system $\mathcal{I}$ the dynamical behavior of these rigid bodies is described by

$$\underbrace{\begin{bmatrix} m_R & 0 \\ 0 & m_R \end{bmatrix}}_{:=\mathbf{M}_R} \ddot{\mathbf{r}}_R + \underbrace{\begin{bmatrix} d_R & 0 \\ 0 & d_R \end{bmatrix}}_{:=\mathbf{B}_R} \dot{\mathbf{r}}_R + \underbrace{\begin{bmatrix} c_R & 0 \\ 0 & c_R \end{bmatrix}}_{:=\mathbf{C}_R} \mathbf{r}_R = m_R e \Omega^2 \begin{pmatrix} \cos(\Omega t) \\ \sin(\Omega t) \end{pmatrix} + \mathbf{F}_f(\Delta\mathbf{r}) \quad (1)$$

and

$$\underbrace{\begin{bmatrix} m_S & 0 \\ 0 & m_S \end{bmatrix}}_{:=\mathbf{M}_S} \ddot{\mathbf{r}}_S + \underbrace{\begin{bmatrix} d_S & 0 \\ 0 & d_S \end{bmatrix}}_{:=\mathbf{B}_S} \dot{\mathbf{r}}_S + \underbrace{\begin{bmatrix} c_S & 0 \\ 0 & c_S \end{bmatrix}}_{:=\mathbf{C}_S} \mathbf{r}_S = -\mathbf{F}_f(\Delta\mathbf{r}) \quad (2)$$

where

$$\Delta\mathbf{r} = \mathbf{r}_R - \mathbf{r}_S \quad (3)$$

and $\dot{(.)} = \frac{\mathrm{d}}{\mathrm{d}t}(.)$ is the derivative with respect to time $t$. The influence of gravitational forces is not considered. $\mathbf{F}_f(\Delta\mathbf{r})$ is the fluid force vector which originates from the third part: an incompressible, newtonian lubrication film. The flow is assumed to be fully turbulent at all times due to the axial pressure drop over the seal and the rotor rotation. The fluid force is described by the non-linear *Muszynska* model

$$\mathbf{F}(\Delta\mathbf{r}) = -\begin{bmatrix} m_f & 0 \\ 0 & m_f \end{bmatrix} \Delta\ddot{\mathbf{r}} - \begin{bmatrix} D_f & 2\tau_f\Omega m_f \\ -2\tau_f\Omega m_f & D_f \end{bmatrix} \Delta\dot{\mathbf{r}} - \begin{bmatrix} K_f - m_f\tau_f^2\Omega^2 & \tau_f\Omega D_f \\ -\tau_f\Omega D_f & K_f - m_f\tau_f^2\Omega^2 \end{bmatrix} \Delta\mathbf{r}. \quad (4)$$

The nonlinearity originates from the terms

$$K_f = K_{f0}(1 - \frac{1}{C}\|\mathbf{r}_R - \mathbf{r}_S\|^2)^{-n}, \quad (5)$$

$$D_f = D_{f0}(1 - \frac{1}{C}\|\mathbf{r}_R - \mathbf{r}_S\|^2)^{-n} \quad (6)$$

and

$$\tau_f = \tau_{f0}(1 - \frac{1}{C}\|\mathbf{r}_R - \mathbf{r}_S\|^2)^{b}. \quad (7)$$

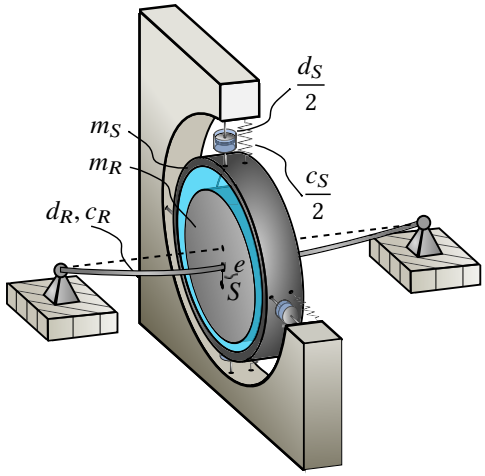


**Figure 1.** Minimal model: *Jeffcott*-rotor and stiff seal ring (visco-elastically connected to its surrounding). An incompressible turbulent fluid flows axially through the sealing gap.

The dependencies of $\mathbf{F}_f$ on the relative rotor deflection $\Delta\mathbf{r}$ and the angular speed $\Omega$ are postulated by the *Muszynska* model. The remaining parameters $m_f$, $D_{f0}$ and $K_{f0}$ are determined using *Childs* analytical formulas for incompressible fluid forces in short plain seals [1]. These formulas are derived from *Hirs'* bulk flow theory which is based on a semi-empirical approach [19]. *Hirs* did experimental validations which showed good agreement of his model for an axial *Reynolds*-number $R_a = \frac{\rho V C}{\mu} < 10^5$ and satisfactory agreement for a circumferential *Reynolds*-number $R_c = \frac{\rho R \Omega}{\mu} < 10^5$. These conditions are met at a dimensionless angular speed of $\eta = \frac{\Omega}{\omega_R} \approx 30$ which will be the maximum speed for all subsequent investigations. *Muszynska*s coefficient form model was motivated by experimental and numerical investigations as well as heuristical considerations. The model is based on the idea that the fluid rotates with a mean circumferential speed of $0 \ll \tau_f\Omega < \frac{1}{2}\Omega$, where $\tau_f = \frac{1}{2}$ is the radial mean value of a perfect laminar *Couette*-flow. The quantity $\tau$ is deflection-dependent. In addition, the rotor vibrations are required to be small enough for the circumferential flow to remain unidirectional (no backward flow) and the whole flow must be temporally fully developed [20]. Considering equations (5) and (6) it becomes apparent, that the fluid stiffness $K_f$ and the fluid damping $D_f$ tend to infinity when the normed relative rotor deflection $\varepsilon = \frac{1}{C}\|\mathbf{r}_R - \mathbf{r}_S\|$ approaches 1, since $n = 2$ was assumed. This modeling does not permit for rotor seal contact, which is of course physically possible. Thus, it must

always be assured that the normed relative deflection does not take on values close to 1. Since the *Muszynska* model is generic, the parameters could also be fitted to represent compressible fluid behavior, which was done in [21].
Combining equations (1) and (2) into one formula gives

$$\overbrace{\begin{bmatrix}\mathbf{M}_R+\mathbf{M}_f & -\mathbf{M}_f\\ -\mathbf{M}_f & \mathbf{M}_S+\mathbf{M}_f\end{bmatrix}}^{:=\mathbf{M}}\ddot{\mathbf{r}}+\overbrace{\begin{bmatrix}\mathbf{B}_R+\mathbf{B}_f & -\mathbf{B}_f\\ -\mathbf{B}_f & \mathbf{B}_S+\mathbf{B}_f\end{bmatrix}}^{:=\mathbf{B}(\Delta\mathbf{r})}\dot{\mathbf{r}}+\underbrace{\begin{bmatrix}\mathbf{C}_R+\mathbf{C}_f & -\mathbf{C}_f\\ -\mathbf{C}_f & \mathbf{C}_S+\mathbf{C}_f\end{bmatrix}}_{:=\mathbf{C}(\Delta\mathbf{r})}\mathbf{r}=m_R e\Omega^2\begin{bmatrix}\cos(\Omega t)\\ \sin(\Omega t)\\ 0\\ 0\end{bmatrix},\quad(8)$$

with

$$\mathbf{r}=(\mathbf{r}_R^\top,\ \mathbf{r}_S^\top)^\top \tag{9}$$

and $\mathbf{B}(\Delta\mathbf{r})$ or $\mathbf{C}(\Delta\mathbf{r})$ respectively being non-linearly dependent on the relative deflection $\Delta\mathbf{r}$ due to the fluidic part.

This contribution is considering an unbalanced rotor, which makes it favorable to rewrite equations (8) with respect to a rotor co-rotating cartesian frame of reference $\mathcal{R}$ and co-rotating coordinates

$$\mathbf{r}_R=\mathbf{R}\,\mathbf{q}_R, \tag{10}$$

and

$$\mathbf{r}_S=\mathbf{R}\,\mathbf{q}_S \tag{11}$$

where

$$\mathbf{R}=\begin{bmatrix}\cos(\Omega t) & -\sin(\Omega t)\\ \sin(\Omega t) & \cos(\Omega t)\end{bmatrix}. \tag{12}$$

Inserting equations (10) to (12) into equations (8) gives

$$\mathbf{M}\ddot{\mathbf{q}}+[\mathbf{B}(\Delta\mathbf{q})-2\Omega\mathbf{Q}\mathbf{M}]\,\dot{\mathbf{q}}+\left[\mathbf{K}(\Delta\mathbf{q})-\Omega\mathbf{Q}\mathbf{B}(\Delta\mathbf{q})-\Omega^2\mathbf{M}\right]\mathbf{q}=m_R e\Omega^2\begin{pmatrix}1\\0\\0\\0\end{pmatrix} \tag{13}$$

with

$$\mathbf{Q}=\begin{bmatrix}\left[\begin{smallmatrix}0&1\\-1&0\end{smallmatrix}\right] & \mathbf{0}\\ \mathbf{0} & \left[\begin{smallmatrix}0&1\\-1&0\end{smallmatrix}\right]\end{bmatrix} \tag{14}$$

and

$$\mathbf{q}=(\mathbf{q}_R^T,\ \mathbf{q}_S^T), \tag{15}$$

which is valid since $\|\mathbf{r}_R-\mathbf{r}_S\|^2=\|\mathbf{q}_R-\mathbf{q}_S\|^2$ holds. The results are autonomous differential equations.

## 3. RESULTS

In the following three subsections the results of the numerical investigation of equations (8) and (13) are presented. All results were obtained by using MATLAB® and the continuation toolbox MATCONT. The main focus of this contribution is the stability and bifurcation behavior of the system under the influence of unbalance. The results for a rotor with an exemplary unbalance of $e=0.15\,C$ will be contrasted with results of an equally unbalanced rotor with stiff seal foundation and a balanced rotor with visco-elastic seal foundation, thereby illustrating the effect of unbalance and support compliance. All results of the bifurcation analysis are visualized with respect to the co-rotating reference frame $\mathcal{R}$. Synchronized periodic limit cycles with respect to the inertial frame $\mathcal{I}$ become equilibria positions with respect to $\mathcal{R}$ and quasi-periodic motions become periodic ones. Consequently, the terminology in this section refers to reference frame $\mathcal{R}$ followed by the corresponding terms with respect to $\mathcal{I}$ in brackets. The depiction of the results solely by means of radii is complete since only circular orbits occur due to the geometrical symmetry of the structure of the system.

### 3.1 Stability analysis

In practice, ever-present unbalance leads to periodic (synchronized) limit cycles. These cycles can become unstable with increasing rotor speed resulting in potentially harmful quasi-periodic vibrations. This is also known as oil whirl phenomena. The stability of periodic limit cycles can be investigated by applying *Floquet* theory. By switching to co-rotating coordinates $\mathbf{q}_{R,S}$ and reference frame $\mathcal{R}$ the stability analysis simplifies to the calculation of eigenvalues of equations (13) linearized around the current equilibrium position $\mathbf{q}_0$ (periodic limit cycle (PLC)) given by

$$\left(\mathbf{K}(\Delta\mathbf{q}_0)-\Omega\mathbf{Q}\mathbf{B}(\Delta\mathbf{q}_0)-\Omega^2\mathbf{M}\right)\mathbf{q}_0=m_R e\Omega^2\begin{bmatrix}1\\0\\0\\0\end{bmatrix}. \tag{16}$$

Fig. 3 displays the stability behavior of the unbalanced and balanced compliant rotor-seal system (red line/ black line) as well as the unbalanced rotor-stiff seal system (blue line). In this chart the stiffness ratio $\kappa^2=\frac{c_S}{c_R}$ is plotted against the dimensionless angular rotor speed $\eta=\frac{\Omega}{\omega_R}$, where $\omega_R$ as the rotor eigenfrequency does not include liquid effects ($\omega_R$ is also known as dry critical speed). Encircled digits indicate numbers of unstable (complex conjugated) pairs of eigenvalues (*Floquet* Multipliers (FM)) and the letters *A* und *B* correspond to individual unstable pairs. The solid red and black lines mark the stability border, whereas the dashed red lines separate areas of different unstable eigenvalue pairs (FM)[1]. Looking at fig. 3 four major conclusions can be drawn: First, comparing the vertical blue and the red/ black lines shows that added compliance may substantially increase or decrease the stability of the system. For lower stiffness ratios an area of extended stability forms to the right, where higher operational speeds can be reached. At higher $\kappa$ values the stability is diminished. Secondly, the compliance of the seal foundation can be identified as the stabilizing mechanism since the stability boundaries for compliant and stiff support

[1] The same separating lines also exist for the balanced rotor (black line). They are not shown to enhance graphic representation.

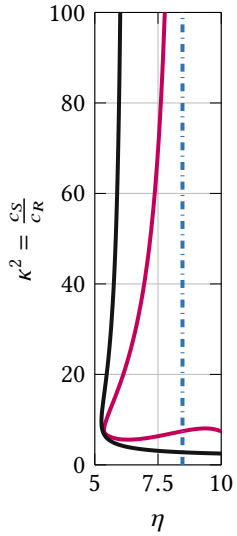


**Figure 2.** Detail from fig. 3

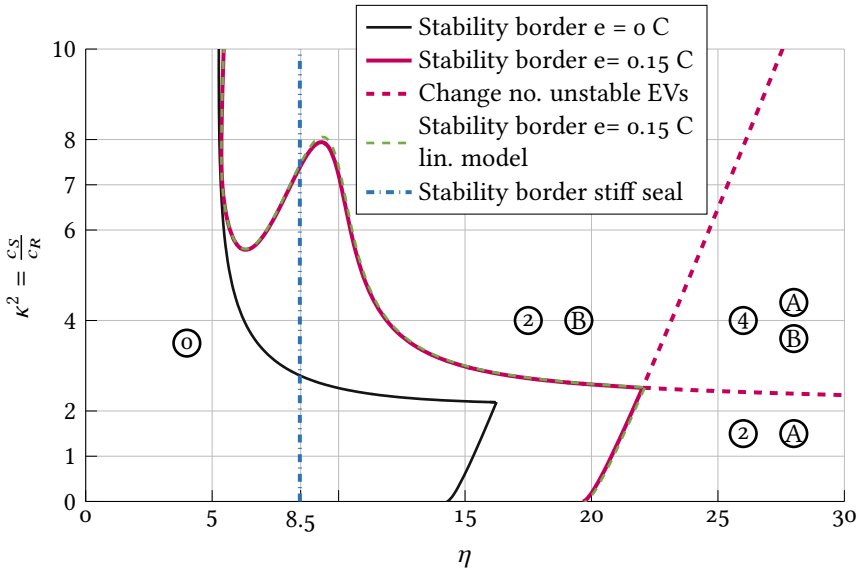


**Figure 3.** Stability chart of equilibria or synchronized PLCs. Encircled digits indicate areas with noted numbers of unstable eigenvalues/ *Floquet* Multipliers; encircled letters *A* and *B* correspond to specific unstable pairs of eigenvalues/ *Floquet* Multipliers.

(blue and red line) converge towards each other for higher $\kappa$ values (cf. fig. 2). Thirdly, the compliant system becomes unstable due to different pairs of eigenvalues (FM) leading to the beneficial or adverse influence of the stiffness ratio $\kappa$ on the stability behavior. Each eigenvalue pair (FM) corresponds to an individual nonlinear behavior which can be seen in the next section. The statement, that support flexibility in general in a system can enhance the stability behavior if designed properly, corresponds qualitatively to the works in [18, 16]. And fourthly, comparing the green dashed line, which represents the stability border for $e = 0.15C$ and a linear force model ($b = n = 0$, cf. eq.(5) - (7)), with its nonlinear counterpart (red solid line) it can be seen that the nonlinearity has no major influence on the stability border.

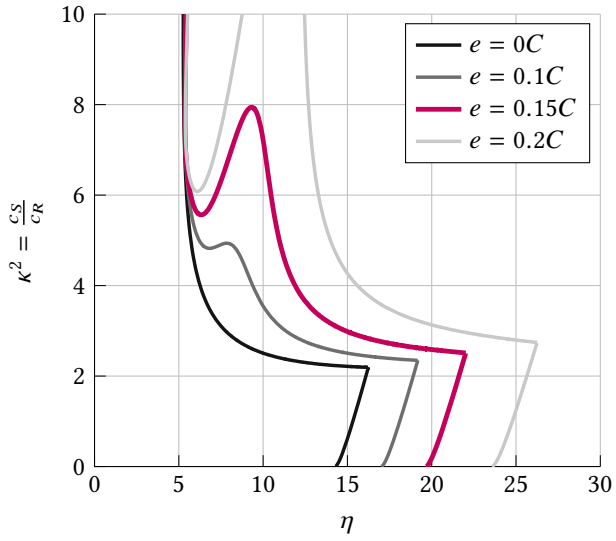


**Figure 4.** Stability chart of equilibria or synchronized PLCs due to different magnitudes of mass eccentricity $e$.

Due to the low deflection of rotor and seal the nonlinear *Muszynska* model is still within linear validity, which is often the case for deflections $< 0.5C$ [13]. In addition to the influence of compliance the effect of unbalance on the system is important. Fig. 4 shows the stability borders for systems with varying unbalance. Two principal effects can be concluded: On the one hand side the area of extended stability is enlarged by increasing unbalance. Similar results for stiff support were also reported by S. Li [14]. Looking more closely at fig. 2 and 3 reveals in contrast that there is also a parameter range $6 < \kappa^2 < 10$ where the unbalance has nearly no influence on the stability at all. On the other hand side, tongues of extended stability form in an upward direction. This special behavior will be discussed in subsection 3.3.

## 3.2 Bifurcation behavior for $\kappa^2 = 1$:

In this section the bifurcation analysis for $\kappa^2 = \frac{c_S}{c_R} = 1$ with respect to the bifurcation parameter $\eta$ is presented. Fig. 6 shows the expected bifurcation diagram of a rotor-seal system with stiff support in dependence of the dimensionless angular rotor speed $\eta$ as the bifurcation parameter.

Here, the solid (dashed) gray line marks stable (unstable) rotor equilibria positions (PLC) $\frac{1}{C}\|\mathbf{q}_R\|$. The blue line indicates the radius $\frac{1}{C}\|\mathbf{q}_R\|$ of stable unsynchronized periodic limit cycles (quasi-periodic attractor (QPA)). After passing through the slightly tilted resonance peak a *Hopf* bifurcation (*Neimark-Sacker* bifurcation (NSB)) occurs which is also known as oil whirl. The fast rising amplitudes soon reach critical levels, where contact between rotor and seal becomes more likely and a safe machine operation is not guaranteed any more. The validity of the quantitative statement of the *Muszynska* model for such high amplitudes must be evaluated with caution. Nevertheless, qualitative conclusions may be drawn. Near $\eta = 25$ a period doubling bifurcation

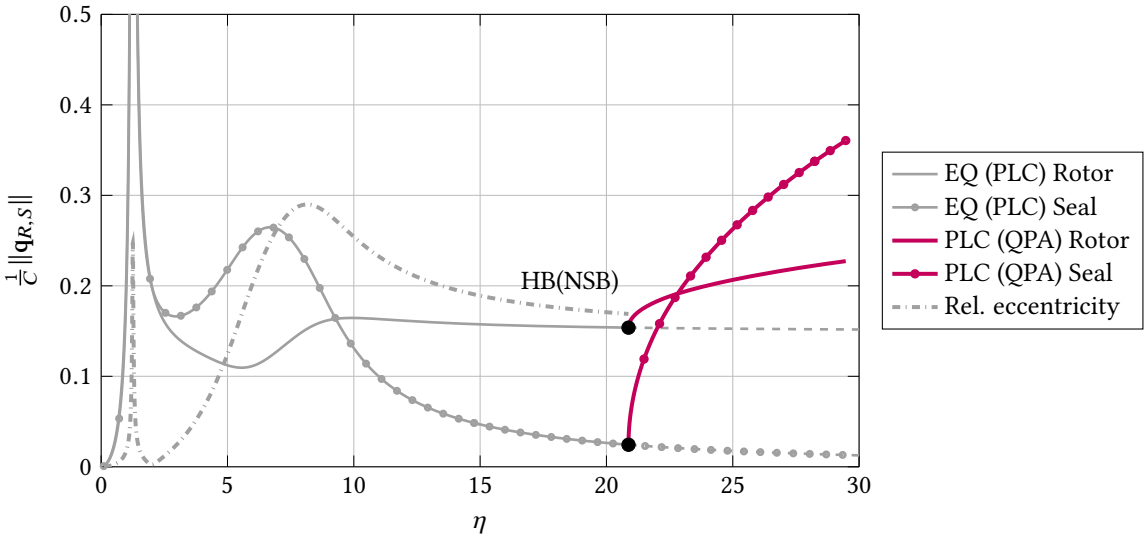


**Figure 5.** Bifurcation path for $\kappa^2 = 1$ and mass eccentricity $e = 0.15\,C$; normed rotor/ seal radii $\frac{1}{C}\|\mathbf{q}_{R,S}\|$ are plotted against $\eta = \frac{\Omega}{\omega_R}$; dashed lines indicate unstable solutions; all results wrt $\mathcal{R}$.

(secondary period doubling bifurcation (SPDB)) occurs.
In addition to the systematic of labeling in fig. 6, dotted lines in fig. 5 correspond to the dynamic behavior of the seal and solid lines to the one of the rotor. The dash-dotted gray line indicates the relative deflection $\frac{1}{C}\|\Delta\mathbf{q}\| = \frac{1}{C}\|\mathbf{q}_R - \mathbf{q}_S\|$ of the rotor.

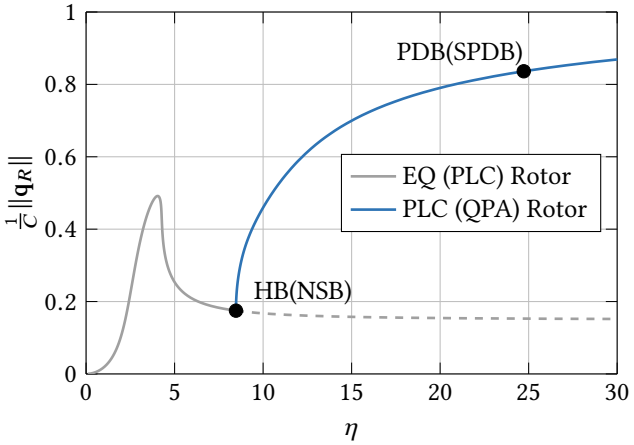


**Figure 6.** Bifurcation path for stiff seal support and mass eccentricity $e = 0.15\,C$;; normed rotor radii $\frac{1}{C}\|\mathbf{q}_R\|$ are plotted against $\eta = \frac{\Omega}{\omega_R}$; dashed line indicates unstable solutions; all results wrt $\mathcal{R}$.

The figure displays a qualitatively and quantitatively completely different picture compared to its stiff counterpart in fig. 6: First of all, the solution shows two resonance peaks within the stable operation range. The in comparison to the stiffly supported seal lower (first) critical speed is not unexpected when adding flexibility to a system and also found in [16]. The passage through this first critical speed 1results in very high amplitudes of rotor and seal with a maximal magnitude of around $\frac{1}{C}\|\mathbf{q}_{R,S}\| \approx 4$. Yet, the relative deflection $\frac{1}{C}\|\Delta\mathbf{q}\| = \frac{1}{C}\|\mathbf{q}_R - \mathbf{q}_S\|$ stays below 0.25. The second resonance only results in higher amplitudes for the seal which is in correspondence with the dominant eigenmode. The course of the relative deflection in the vicinity of and after the second resonance peak can be explained by a change in the phase angle (not shown here) between rotor and seal: first, rotor and seal conduct an in phase-motion which lasts even during the first resonance peak and changes then to a phase difference of around $\frac{2}{3}\pi$. The stability of the equilibrium (PLC) is lost in a *Hopf* bifurcation (NSB) leading to oil whirl motions of rotor and seal, whereas seal amplitudes rise fast and rotor amplitudes rise slow. Three interesting properties become apparent comparing the behavior of stiff and compliant support. First, as already indicated in fig. 3, the onset speed of instability of the compliant system is much higher. It can be operated at higher speeds with stable synchronized and, thus, lower rotor amplitudes. Secondly, the absolute rotor amplitudes in the resonance area of the compliant system are extremely high, but the relative deflection only takes on values which are 50% smaller than the amplitudes of the stiff seal support. A passage without rotor-seal contact through the resonance area is much more likely.

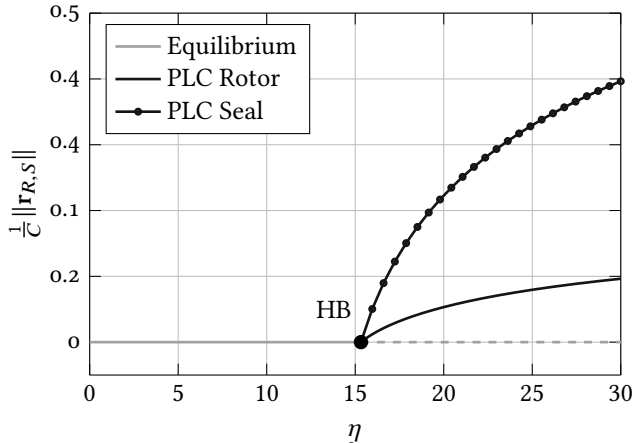


**Figure 7.** Bifurcation path for $\kappa^2 = 1$ and balanced rotor; normed rotor/ seal radii $\frac{1}{C}\|\mathbf{r}_{R,S}\|$ are plotted against $\eta = \frac{\Omega}{\omega_R}$; dashed line indicates unstable solutions; all results wrt $\mathcal{I}$.

Thirdly, the amplitudes of the periodic limit cycles (QPA) after the loss of stability are much smaller for the compliant system. Especially the rotor amplitudes stay considerably small which could make an ongoing operation possible. Oil whip motion does not occur in either of the two systems: with the used parameters and within the considered rotational speed the whirl frequency does not coincide with one of the resonance frequencies.
Fig. 7 shows the bifurcation path for the balanced system. The gray line marks the centric rotor/ seal equilibrium position (wrt $\mathcal{I}$) which looses its stability in a *Hopf* bifurcation. The emerging periodic limit cycles display medium sized seal and small rotor amplitudes. The comparison of the balanced and unbalanced case emphasizes again the statement of fig. 2 that the unbalance stabilizes the solution and leads to higher rotational speeds with stable solutions. Despite starting from different equilibria positions (wrt $\mathcal{R}$ in the unbalanced and wrt $\mathcal{I}$ in the balanced case) both amplitudes show a qualitative similar behavior in dependence of $\eta$.

## 3.3 Bifurcation behavior for $\kappa^2 = 7$:

In this section the bifurcation analysis for $\kappa^2 = \frac{c_S}{c_R} = 7$ with respect to the bifurcation parameter $\eta$ is presented.
The bifurcation behavior of the compliant system with unbalance is shown in fig. 9 and a detail in fig. 8. The chosen path crosses the upwards reaching tongue of extended stability in fig. 3 and shows the excepted rich dynamics. The solution shows five interesting parts separated by *Hopf* bifurcations (NSB) which will be discussed individually:
The first part is the first resonance peak (c.f. fig. 8). The system passes through the resonance with maximal amplitudes of around $\frac{1}{C}\|\mathbf{q}_{R,S}\| \approx 2$. The relative deflection reaches values of $\frac{1}{C}\|\Delta\mathbf{q}\| = \frac{1}{C}\|\mathbf{q}_R - \mathbf{q}_S\| \approx 0.5$ and the tip is slightly bend to the right as expected from systems with noticeable non-linearities. Compared to the bifurcation path for $\kappa^2 = 1$ the maximal amplitudes are lower while the relative deflection $\|\Delta\mathbf{q}\|$ is higher. A possible explanation might be the following: the damping in the seal support is low, whereas the fluid damping is approximately 10 times higher. Keeping in mind that the seal is easier to move for low stiffness ratios $\kappa^2$ it is clear that the process at $\kappa^2 = 1$ is dominated by the low seal damping and low squeezing or energy dissipation respectively by the fluid. There is greater fluid squeezing at high stiffness ratios since the seal is less movable and, thus, large energy dissipation limits the maximum amplitudes[2].

After the decline of the amplitudes a first *Hopf* bifurcation (NSB) occurs which is the second interesting aspect. After the bifurcation the amplitudes of the periodic limit cycles (QPA) rise fast just to loose their stability in a fold bifurcation (secondary fold bifurcation (SFB)). In this small $\eta$ interval the amplitudes rise even higher than in the whole considered $\eta$ interval for $\kappa^2 = 1$. The instability in this instance is caused by the eigenvalue pair $B$ (FM) leading to the qualitatively completely different behavior with rotor and seal amplitudes of similar magnitude. The stability is regained in a second fold bifurcation (SFB) and the resulting stable periodic limit cycle (QPA) collapses in another *Hopf* bifurcation (NSB)[3].
The third part is the area of stable equilibria (PLC) between *Hopf* bifurcation 2 and 3, where the self-excited whirl motion synchronizes with the unbalance induced vibrations in the vicinity of the second resonance. This behavior is also described by *Muszynska* in [12] for a stiff support. A possible explanation might be the increase in fluid damping due to the rising relative deflection in the trail of the second resonance (cf. fig.5), which forces the self-excited vibrations to collapse.
Fig. 9 shows the fourth part: the once regained stability is lost again in a third *Hopf* bifurcation (NSB) leading to periodic limit cycles (QPA) whose amplitudes rise qualitatively similar to the ones discussed in the second part: The same eigenvalue pair $B$ (FM) becomes unstable. Extreme high amplitudes are encountered. Finally, crossing the area of two unstable eigenvalues (FM) to four unstable eigenvalues (cf. fig. 3) enforces a fourth *Hopf* bifurcation (NSB) from which an unstable periodic limit cycle (quasi-periodic repellor QPR) emerges.
Compared to the bifurcation behavior for the stiff seal support (cf. fig. 6) it is unfavorable to operate the rotor for $\kappa^2 = 7$ from a practical point of view: The (relative) deflection in the area of the first resonance is comparable in size, the stability limit is much lower, the amplitudes of the oil whirl are fast rising and considerably bigger and, therefore, most certainly prohibiting ongoing operation.
Comparing the unbalanced to the balanced behavior in fig. 10 shows a lot of qualitative resemblances: After the first *Hopf* bifurcation the balanced systems shows fast rising amplitudes. Crossing the line between 2 and 4 unstable eigenvalues an unstable periodic limit cycles emerges, which qualitatively resembles the one in fig. 7. The periodic limit cycles (QPA) of the unbalanced system display a similar fast rise in amplitudes after *Hopf* bifurcations 1 and 3 (NSB) and a correspondence between the unstable periodic limit cycle (QPA) after *Hopf* bifurcation 4 (NSB) can be seen.

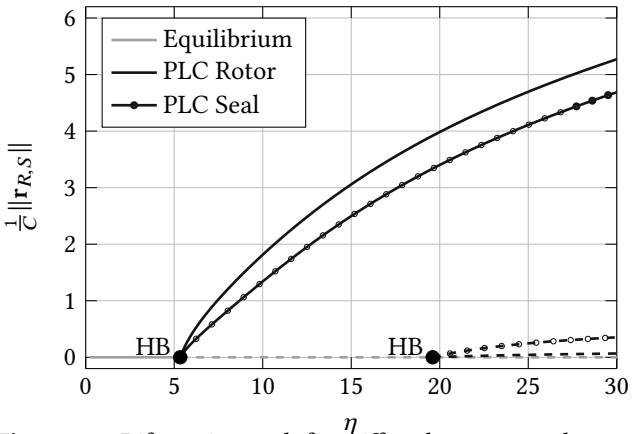


**Figure 10.** Bifurcation path for stiff seal support and a balanced rotor; normed rotor/ seal $\frac{1}{C}\|\mathbf{r}_{R,S}\|$ radii are plotted against $\eta = \frac{\Omega}{\omega_R}$; dashed lines indicate unstable solutions; all results wrt $\mathcal{R}$.

[2] Changing the parameter settings for the simulation will of course lead to a changed dissipation mechanism.

[3] *Hopf* and fold bifurcation are close together and, therefore, not indicated separately in the chart.

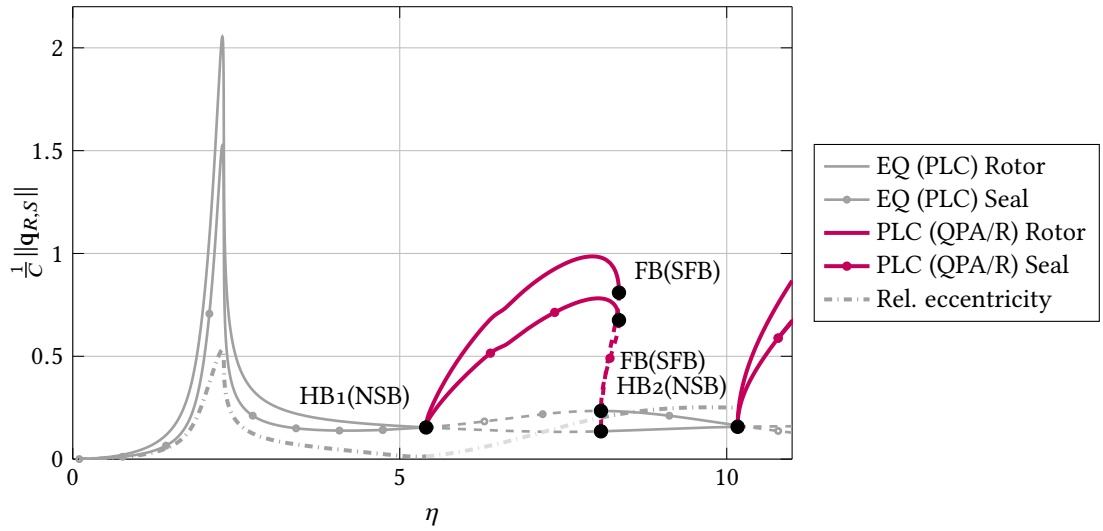


**Figure 8.** Bifurcation path for $\kappa^2 = 7$ and mass eccentricity $e = 0.15\,C$; normed rotor/ seal radii $\frac{1}{C}\|\mathbf{q}_{R,S}\|$ are plotted against $\eta = \frac{\Omega}{\omega_R}$; dashed lines indicate unstable solutions; all results wrt $\mathcal{R}$.

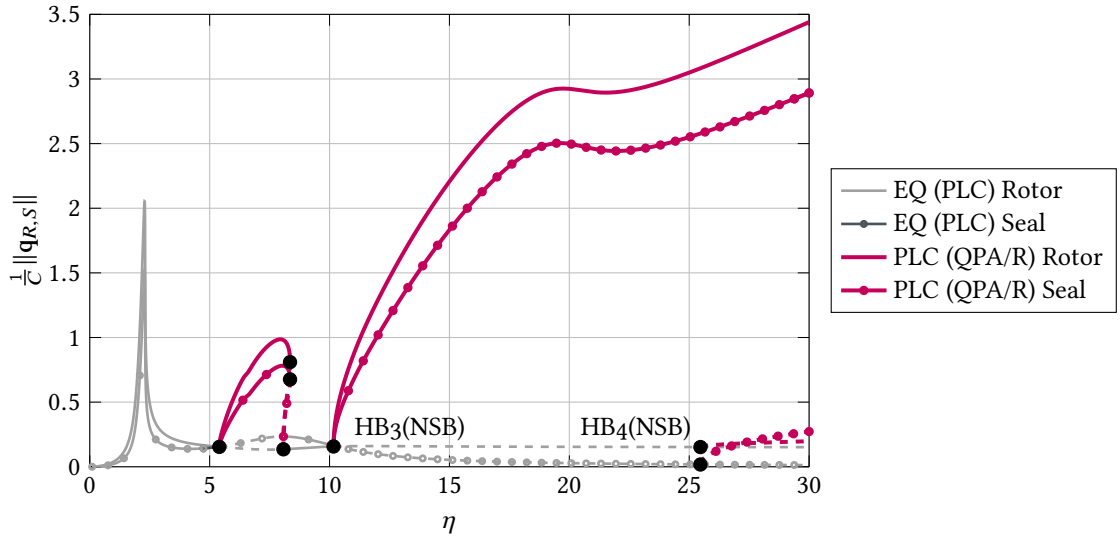


**Figure 9.** Bifurcation path for $\kappa^2 = 7$ and mass eccentricity $e = 0.15\,C$; normed rotor/ seal $\frac{1}{C}\|\mathbf{q}_{R,S}\|$ radii are plotted against $\eta = \frac{\Omega}{\omega_R}$; dashed lines indicate unstable solutions; all results wrt $\mathcal{R}$.

Applications, where the sealing fluids are incompressible such as pumps or sealed fluid film bearings, involve often classically stiff rotors[4], which is not the case for the results presented here. Despite being more of a fundamental study, these results do nevertheless apply to systems which were initially designed to run below critical speed but actually run overcritical or near critical if the flexibility of the surrounding seal structure is taken into account [22]. The results also apply to cases where the compressibility of the gas can be neglected as a first approximation (e.g. liquid fuel turbopump/ liquid hydrogen [18]).

[4] ANSI/ API Standard 610: classically stiff rotors are characterized by a first dry critical speed being 20% - 30% above the continuous machine speed.

## 4. CONCLUSION AND OUTLOOK

Alternatively to the established designs of brush and labyrinth seals, hybrid seal might feature low leakage, low wear and improved rotordynamic properties. This issue has been discussed in this contribution by means of a simple rotor-seal model comprising an unbalanced rotor and a compliant seal support with a focus on incompressible fluids. The fluid forces have been represented by the non-linear *Muszynska* model. The results have been compared to the same model with stiff seal support and to a balanced compliant rotor-seal model.

The enabled movability of the stiff seal ring can increase or decrease the stable operation range depending on the stiffness ratio $\kappa^2 = \frac{c_S}{c_R}$. The stable operation range enlarges and stability tongues form with rising mass eccentricity.

In case of lower stiffness ratios the relative rotor deflection stays small even during resonance passage and subsequent

amplitudes of an oil whirl motion are bounded. This configuration might be suitable for practical use and displays improved properties compared to the stiff support.
Higher stiffness ratios lead to a decreased stable operation range and high whirl amplitudes. The rich occurring bifurcation behavior assigns this case more theoretical than practical relevance: Orbital stability is lost and regained in *Neimark-Sacker* bifurcations leading to quasi-periodic vibrations and resynchronization.
Future work will include three major parts: The non-linear effects of the present model before and after a loss of stability (synchronization, *Arnold* tongues, chaos) will be investigated. This requires a fluid model being valid at higher rotational speeds. In a second part, the understanding of the fluid mechanical interaction with the rotor shall be deepened by building up a fully coupled FEM simulation of *Hirs'* fluid model and incorporating compressible fluid film models. Some yet unpublished work has been conducted in this area. Manufacturing and commissioning of an already designed test rig is the last major part.

## REFERENCES


[1] Dara W Childs. Dynamic analysis of turbulent annular seals based on hirs' lubrication equation. *Journal of Lubrication Technology*, 105(3):429–436, 1983.

[2] Luis San Andrés and Alain Anderson. An all-metal compliant seal versus a labyrinth seal: A comparison of gas leakage at high temperatures. *Journal of Engineering for Gas Turbines and Power*, 137(5):052504, 2015.

[3] Dara W Childs. *Turbomachinery rotordynamics: phenomena, modeling, and analysis*. John Wiley & Sons, 1993.

[4] MJ Braun and VV Kudriavtsev. A numerical simulation of a brush seal section and some experimental results. In *ASME 1993 International Gas Turbine and Aeroengine Congress and Exposition*, pages V03CT17A059–V03CT17A059. ASME, 1993.

[5] AD Dimarogonas. Newkirk effect: thermally induced dynamic instability of high-speed rotors. In *ASME 1973 International Gas Turbine Conference and Products Show*, pages V001T01A026–V001T01A026. ASME, 1973.

[6] Andrew Messenger, Richard Williams, Grant Ingram, Simon Hogg, Stacie Tibos, and Jon Seaton. A dynamic clearance seal for steam turbine application. In *ASME Turbo Expo 2015*, pages V008T26A031–V008T26A031. ASME, 2015.

[7] BL Newkirk. Shaft whipping. *General Electric Review*, 27(3):169–178, 1924.

[8] FS Bedcher and AA Lomakin. Determination of the critical number of revolutions of a pump rotor with a view to the forces induced in the seals. In *Construction of Steam and Gas Turbines*, number 5, pages 249–269, 1957.

[9] Chung-Wah Ng and CHT Pan. A linearized turbulent lubrication theory. *Journal of Basic Engineering*, 87(3):675–682, 1965.

[10] VN Constantinescu. The pressure equation for turbulent lubrication. In *Proceedings of the Conference on Lubrication and Wear*, volume 182, page 183. IMechE, 1967.

[11] Gilles Gerardus Hirs. A bulk-flow theory for turbulence in lubricant films. *Journal of Lubrication Technology*, 95(2):137–146, 1973.

[12] Agnes Muszynska. Whirl and whip – rotor/bearing stability problems. *Journal of Sound and vibration*, 110(3):443–462, 1986.

[13] Q Ding, JE Cooper, and AYT Leung. Hopf bifurcation analysis of a rotor/seal system. *Journal of Sound and Vibration*, 252(5):817–833, 2002.

[14] Li Song-tao, Xu Qing-yu, Wan Fang-yi, and Zhang Xiao-long. Stability and bifurcation of unbalance rotor/labyrinth seal system. *Applied Mathematics and Mechanics*, 24(11):1290–1301, 2003.

[15] Wei Li, Yi Yang, Deren Sheng, and Jianhong Chen. A novel nonlinear model of rotor/bearing/seal system and numerical analysis. *Mechanism and Machine Theory*, 46(5):618–631, 2011.

[16] José A Vaázquez, Lloyd E Barrett, and Ronald D Flack. A flexible rotor on flexible bearing supports: stability and unbalance response. *Journal of Vibration and Acoustics*, 123(2):137–144, 2001.

[17] Zenglin Guo and R Gordon Kirk. Instability boundary for rotor-hydrodynamic bearing systems, part 2: rotor with external flexible damped support. *Journal of Vibrations and Acoustics*, 125(4):423–426, 2003.

[18] Changqing Bai, Qingyu Xu, and Jiyan Wang. Effects of flexible support stiffness on the nonlinear dynamic characteristics and stability of a turbopump rotor system. *Nonlinear Dynamics*, 64(3):237–252, 2011.

[19] Gilles Gerardus Hirs. *Fundamentals of a bulk-flow theory for turbulent lubricant films*. PhD thesis, 1970.

[20] A Muszynska. Improvements in lightly loaded rotor/bearing and rotor/seal models. *Journal of Vibration and Acoustics*, 110(2):129–136, 1988.

[21] Zhong-gang Li and Yu-shu Chen. Research on 1: 2 subharmonic resonance and bifurcation of nonlinear rotor-seal system. *Applied Mathematics and Mechanics*, 33(4):499–510, 2012.

[22] R Gasch. Vibration of large turbo-rotors in fluid-film bearings on an elastic foundation. *Journal of Sound and Vibration*, 47(1):53–73, 1976.